Supplementary Materials for

Physiological and ecological drivers of early spring blooms of a coastal phytoplankter

Kristen R. Hunter-Cevera, Michael G. Neubert, Robert J. Olson, Andrew R. Solow, Alexi Shalapyonok, Heidi M. Sosik*

*Corresponding author. Email: hsosik@whoi.edu

Published 21 October 2016, *Science* **354**, 326 (2016)
DOI: 10.1126/science.aaf8536

This PDF file includes:

Supplementary Material:

Materials and Methods:

Study site

The Martha's Vineyard Coastal Observatory is a cabled facility that consists of a shore-based station and meteorological mast, an undersea node located at 12 m depth, and a tower structure in 15 m water rising 10 m above sea level. The node is located 1.5 km south of the island (41 °20.19'N 70° 33.38' W) and the tower is located 3 km offshore (41°19.5' N 70° 34.0' W). FlowCytobot (FCB) is deployed at 4 m mean water depth at the offshore tower. Deployments from 2003 to 2007 were conducted with only one instrument, but after 2007, with the availability of a second FCB, data were obtained from alternating deployments of each instrument. Core measurements at the MVCO facility include a broad range of meteorological and hydrographic data. Measurements of incident radiation are made at the meteorological mast with an Eppley pyranometer and 20-minute resolution data were downloaded from ftp://mvcodata.whoi.edu/pub/mvcodata/. For the majority of 2010, light data were unavailable, and this data gap was filled with radiation measurements obtained from a NOAA National Buoy Data Center buoy (station 44008), located southeast from Nantucket (40° 30'9" N 69°14'48" W, ~144 km from MVCO). Daily solar radiation was calculated by integrating incident radiation over 24 hours. Temperature was measured continuously at 4 m at the tower with a MicroCat CTD (Seabird Electronics). Data gaps in this record were filled with regression-adjusted temperature measurements taken at the 12-m node (also downloaded from ftp://mvcodata.whoi.edu/pub/mvcodata). Linear regressions used in the correction were calculated for each month. These records have been previously shown to be very similar (*31*).

Near surface water samples were collected bimonthly-to-monthly for nutrient analysis. Samples were immediately filtered through a 0.2 μm Sterivex® filter into acid-washed vials and frozen at -20 °C. Phosphate, ammonium, silicate and nitrate + nitrite concentrations were determined by standard autoanalyzer techniques at the Woods Hole Oceanographic Institution Nutrient Analytical Facility (Woods Hole, MA).

FlowCytobot

The design and performance of FlowCytobot (FCB) are described elsewhere (*11*). Briefly, the instrument uses a 532-nm solid state laser for excitation and is able to detect individual cell

forward and side light scattering and fluorescence at 575 and 680 nm. Data analysis and enumeration of *Synechococcus* cells were as described in (*33*). *Synechococcus* are discriminated from other phytoplankton and particles by their characteristic orange fluorescence from phycoerythrin and small light scattering signals. Cell volumes were estimated from measured side scattering, following the calibration as in (11). Polystyrene microspheres (beads) (Polysciences Inc.) of diameter 0.5 μm (polychromatic) and 1.0 μm (red-fluorescing) were measured as reference particles every ~ 20 h during deployments.

Division rate estimation

We use a matrix population model that represents the diel changes in cell size distribution of *Synechococcus* cells to estimate an in situ, daily population division rate. Briefly, cells are binned into discrete size (volume) classes and within a model time step (10 min), cells may grow into the next size class, divide into a smaller size class or remain in the same class. Cell growth is dependent on incident radiation, and cell division depends on size class. We also specify a starting cell size distribution. We estimate parameters for these functions that best represent daily observations of cell size distributions with a maximum likelihood approach. With maximum likelihood estimates of the parameters, we keep track of all model cells produced from the division function and calculate a division rate from the starting and ending numbers of model cells.

Division rate was estimated with the two-subpopulation model described in (*4*), with a slight difference in model construction. In this model, the variance of the initial cell size distribution is the same for both subpopulations. Here, we have allowed each initial subpopulation size distribution to have its own variance, resulting in an additional model parameter, for a total of 14 estimated parameters. We estimated the parameters for each day via maximum likelihood, assuming a Dirichlet multinomial distribution (*17*). We utilize a constrained nonlinear optimization routine (fmincon) offered in MATLAB (r2016a). Due to the complexity of the parameter space, we initialized the solver with at least 40 random starting points. Best fit parameter values were chosen if they satisfied the following criteria: 1) At least 5 solver runs resulted in parameter estimates for which the maximum likelihood did not differ by more than 0.2, and 2) parameter estimates themselves did not differ by more than 5% or were within a specified absolute error tolerance (please see code and documentation at https://github.com/khuntercevera/phyto-division-rate-model for more information). If the initial starting points did not result in parameter estimates that satisfied

these criteria, another 40 random start points were chosen for up to 200 solver runs. Parameters resulting in the maximum likelihood estimate were then used to calculate a division rate as described in (*17*). We further utilized temperature as a quality constraint for division rate estimates; if estimates were biologically infeasible or highly unlikely given the ambient temperature, these estimates were excluded from the analysis.

Net growth and loss rate calculation

We calculated net growth rate, $\mu_{net}(t)$, from smoothed cell concentration data (48-hour running mean to reduce tidal and other high frequency affects), as follows:

$$\mu_{net}(t) = \ln \frac{\bar{N}(t_d+24)}{\bar{N}(t_d)},$$

where t_d is dawn hour of each day, and $\bar{N}(t_d) = \frac{1}{3}\sum_{j=-1}^{j=1} N(t_d + j)$, where N(t) is the smoothed cell concentration at hour t. $\bar{N}(t_d)$ gives an average cell concentration in the 3-hour interval surrounding dawn to avoid spuriously high or low net growth rates based on choice of hour. The time period for calculating net growth rate matches the time period used for division rate estimation. Loss rates were calculated by subtracting net growth rate from division rate for each day available in the dataset.

Detection of spring bloom shift

Determining when the spring bloom stops and starts for each year is a notoriously difficult problem, and there is no one agreed upon metric (*34*). Here we used the year day at which *Synechococcus* cell concentration last crossed a predetermined threshold level as an indicator of bloom timing and progression (Fig. S1). To evaluate whether our conclusions were sensitive to threshold choice, we considered multiple values.

We computed an integrated division rate as a metric of population growth potential by calculating the quantity $\int_{85}^{200} \mu(t)dt$ as a function of t (year day), for *t* between 85 and 200. This quantity is equal to ln[*N**(200)/*N**(75)], where *N**(*t*) is what the population density would be if there were no losses, only the observed cell division rates. For missing values, the median calculated from a 15-day window surrounding the missing day was used instead (Fig. S7).

To detect shifts in division rate, we identify the year day at which integrated division rate last crossed arbitrary values (4, 12, 24, and 36) during the spring. We similarly computed integrated

loss rates and threshold crossings. These integrated rates are less affected by the inherent day-to-day noise in division and loss rates. The start day of integration did not affect patterns of year day crossings (Fig. S8). For each set of year day threshold crossings, we fit piecewise linear models (inflection point at 2012) between year day crossings and year (MATLAB r2016a).

Supplementary Figures:

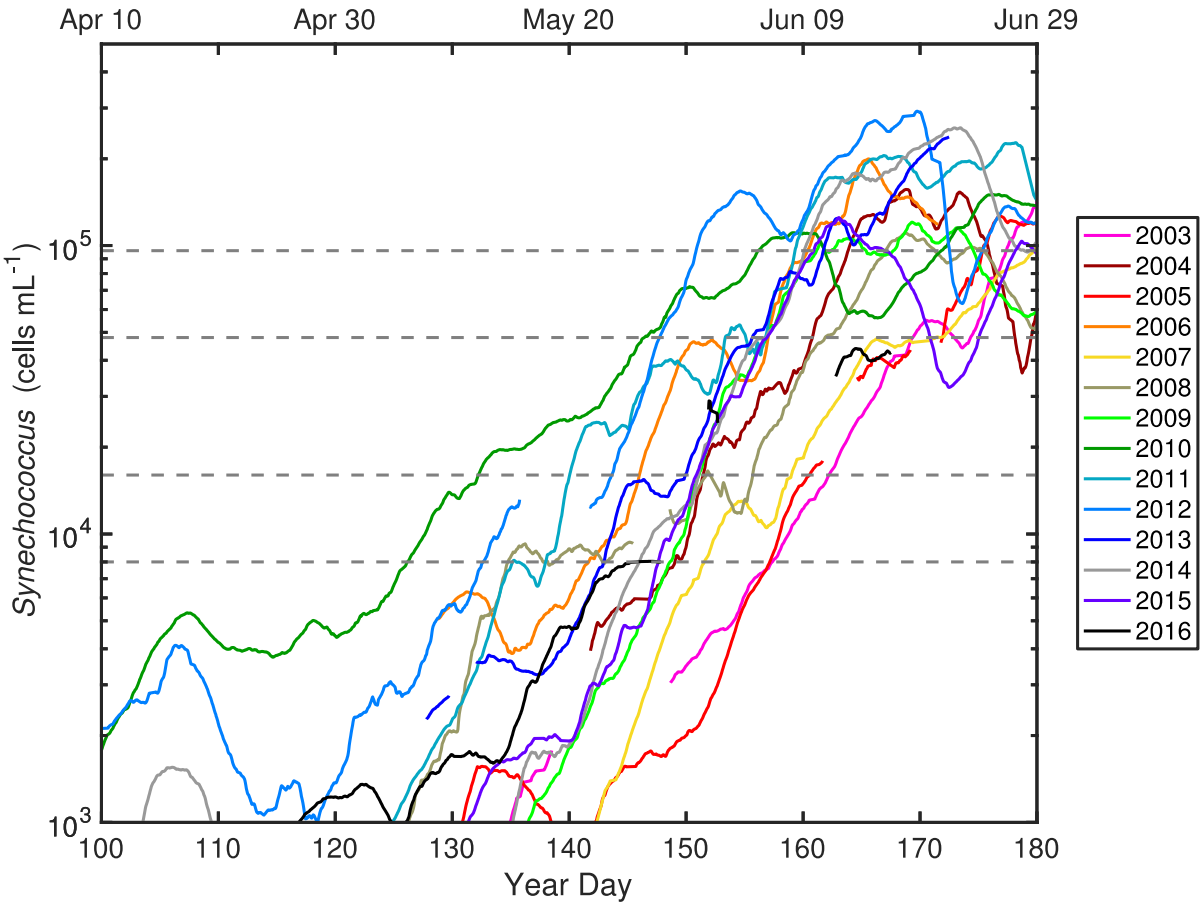

Figure S1. Smoothed (48-hour running mean) *Synechococcus* concentration during the spring bloom for year day 100 to 180. Color indicates year. Gray lines indicate threshold values characteristic of spring bloom ($8 \cdot 10^3$, $1.6 \cdot 10^4$, $4.8 \cdot 10^4$ and $9.6 \cdot 10^5$ cells mL^{-1}).

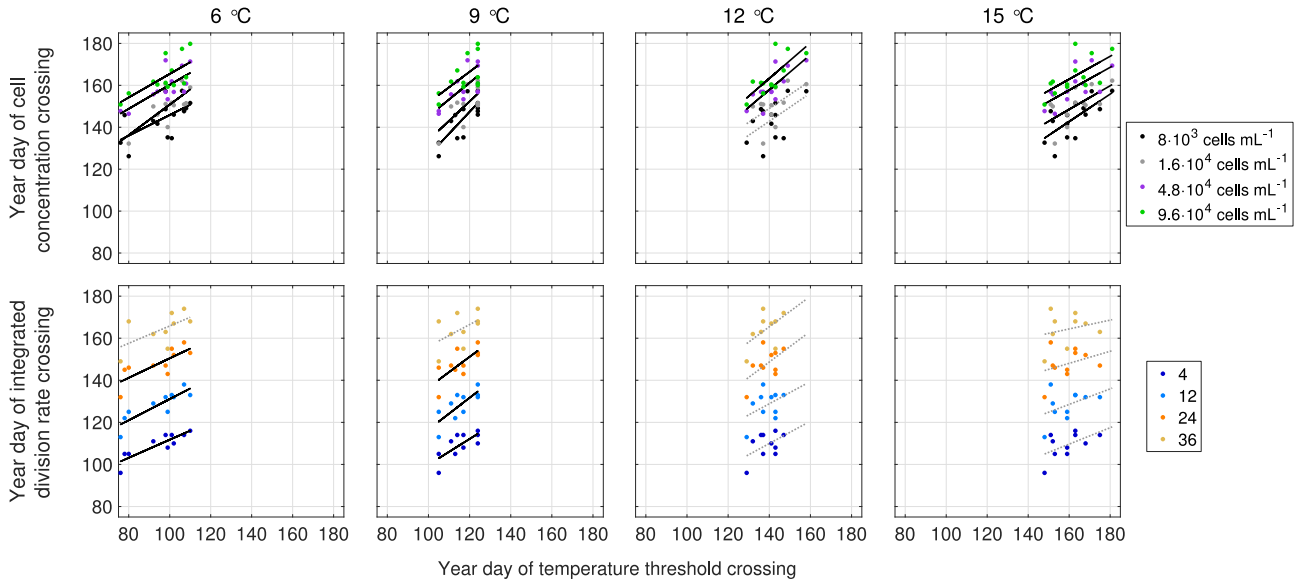

Figure S2. Top panels show relationships between the year day when water temperature first exceeds 6, 9, 12, or 15 °C (one temperature per panel) and the year day when *Synechococcus* first exceeds concentrations of $8{\cdot}10^3$ (black), $1.6{\cdot}10^4$ (gray), $4.8{\cdot}10^4$ (dark green), or $9.6{\cdot}10^4$ cells mL^{-1} (teal) for each year. Bottom panels show relationships between the year day when water temperature first exceeds the same thresholds as top panels and year day when the integrated division rate first exceeds values of 4 (blue), 12 (light blue), 24 (orange) or 36 (gold) for each year. Black lines indicate linear regression fits with slopes significantly different from 0, while gray dotted lines are regression fits without significant slopes. Note the same positive trend regardless in all panels, supporting a systematic role of temperature governing division rate and bloom dynamics.

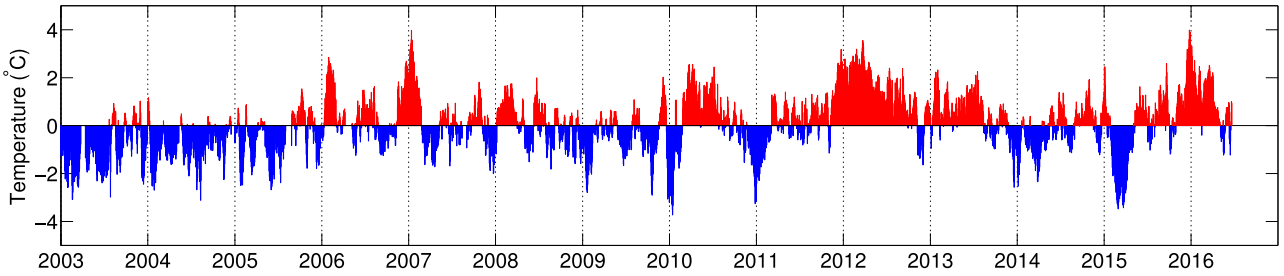

Figure S3. Daily temperature anomalies (ºC) from daily climatological average for 2003 to available 2016. Red values indicate positive anomalies, while blue indicates negative anomalies.

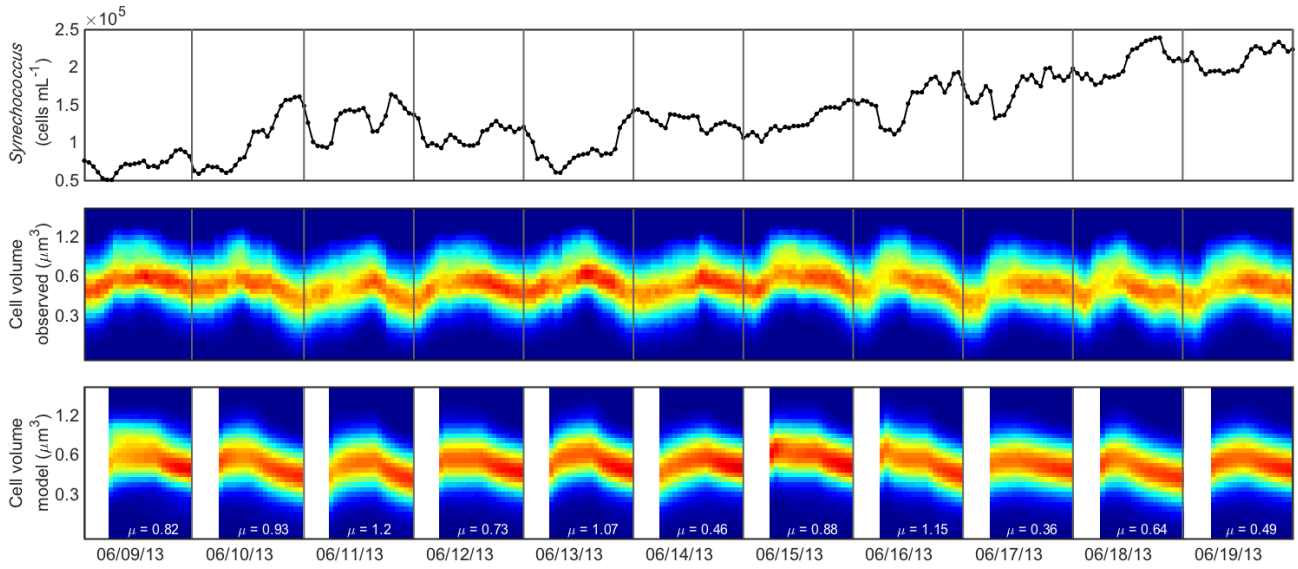

Figure S4. Top panel shows hourly concentration of *Synechococcus* from 9 June – 19 June 2013. Gray vertical lines indicate dawn of each day. Middle panel is corresponding cell size distributions. Bottom panel shows model cell size distributions from maximum likelihood estimates of parameters. Estimated division rate is denoted by μ. Note that model starts 6 hours after dawn, denoted by white space. Color indicates fraction of cells in discrete size classes within an hour. Note that high variation in the size distribution over the day is typically indicative of a high division rate, but this is often not accompanied by a net increase in cell concentration.

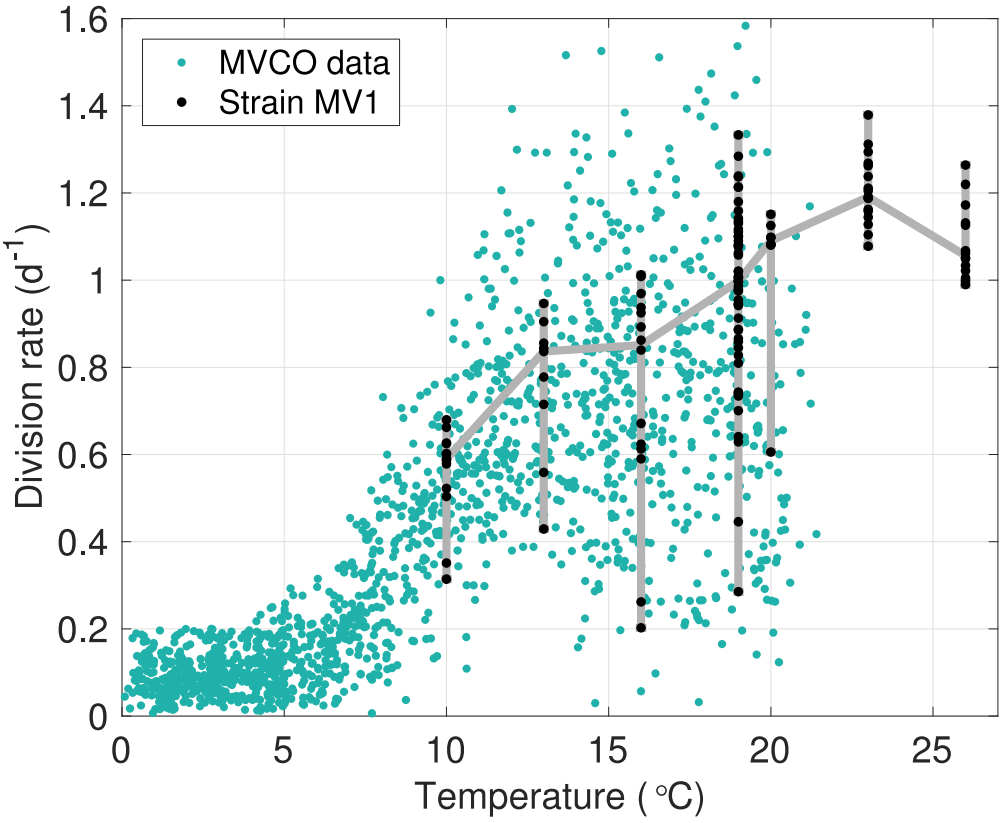

Figure S5. Relationship between division rates and temperature for a cultured *Synechococcus* isolate (strain MV1) from MVCO belonging to the dominant clade I genotype (black dots) and for field estimates between Jan 1 and June 30 for the entire time series (teal dots). Grey lines highlight range of cultured isolate division rates for a given temperature. Culture growth data is from Hunter-Cevera et al. 2014, where details of experiments can be found. These points correspond to a culture grown at 7 different temperatures in semi-continuous batch culture at 80 µmol/m^2/s^2 light.

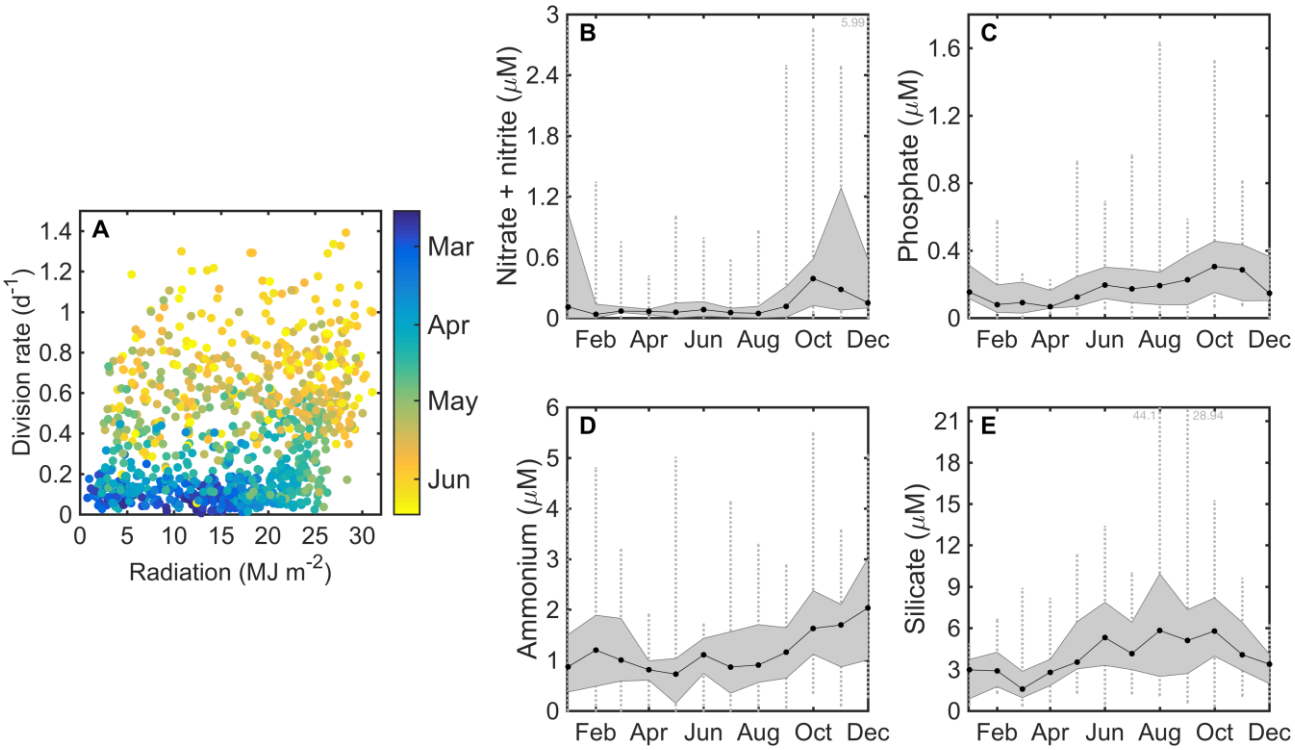

Figure S6. A. Daily division rate estimates and incident radiation (MJ m^2) for spring data for all years in dataset. We find no relationship between division rate and incident radiation during the spring. Monthly median values of nutrient concentration (μM, total of 207 samples). Shaded region encompasses 25th to 75th percentiles, with dotted lines encompassing total range (except for a few values out of plot range, in which case values are printed next to line). B. Nitrate+nitrite C. Phosphate D. Ammonium E. Silicate. Note that during spring, nitrate+nitrate, phosphate and ammonium concentrations remain, on average, relatively constant, suggesting that the increase of division rate is not driven by these nutrients.

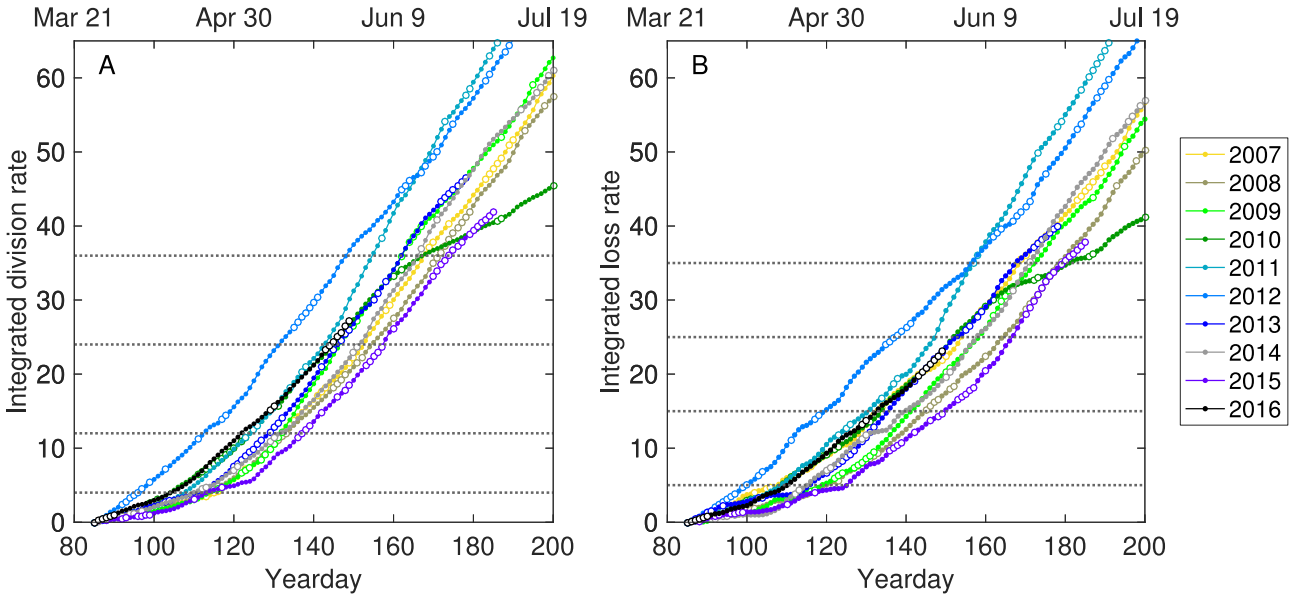

Figure S7. A. Integrated division rate from year day 85 to 200. B. Integrated loss rate for same time period as in A. Color denotes year. Open circles indicate missing data, which was filled using a 15-day window median value surrounding missing day. Dotted lines indicate arbitrary threshold values (4, 12, 24, 36) used in Figure 2.

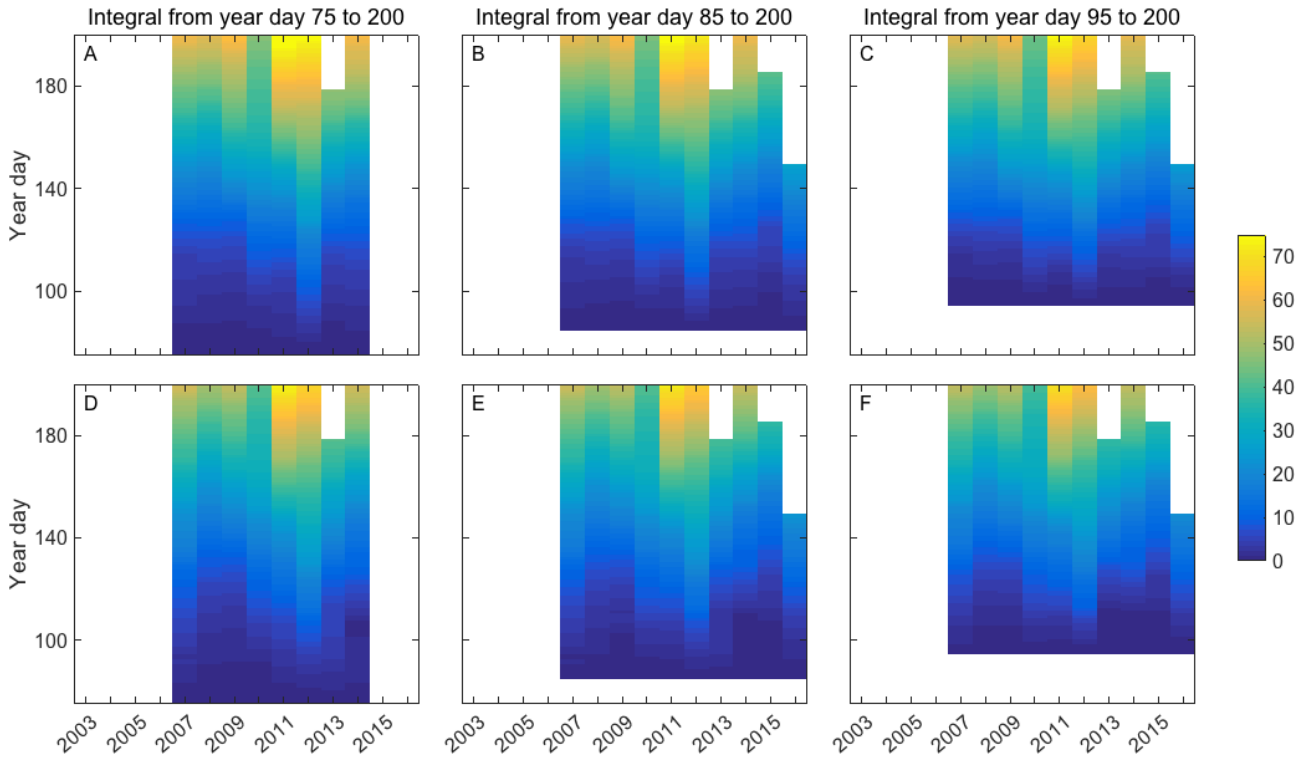

Figure S8. Top panels: cumulative integrated division rate starting at different year days for each year from 2007-2016 denoted by color. A. Year day 75. B. Year day 85. C. Year day 95. Bottom panels: cumulative integrated loss rate starting at different year days for each year from 2007-2016 denoted by color. D. Year day 75. E. Year day 85. F. Year day 95. Integrations are missing for 2015 and 2016 starting at year day 75 as not enough data was unavailable before this start day to begin the integration. Note that patterns starting at different year days are very similar, such that analysis appears insensitive of this arbitrary start day for integration as well as arbitrary integration thresholds.

References and Notes

1. K. R. Arrigo, D. Worthen, A. Schnell, M. P. Lizotte, Primary production in Southern Ocean waters. *J. Geophys. Res. Oceans* **103**, 15587–15600 (1998). doi:10.1029/98JC00930

2. P. Martin, R. S. Lampitt, M. Jane Perry, R. Sanders, C. Lee, E. D'Asaro, Export and mesopelagic particle flux during a North Atlantic spring diatom bloom. *Deep Sea Res. Part I Oceanogr. Res. Pap.* **58**, 338–349 (2011). doi:10.1016/j.dsr.2011.01.006

3. R. Ji, M. Edwards, D. L. Mackas, J. A. Runge, A. C. Thomas, Marine plankton phenology and life history in a changing climate: Current research and future directions. *J. Plankton Res.* **32**, 1355–1368 (2010). Medline doi:10.1093/plankt/fbq062

4. K. H. Wiltshire, A. Kraberg, I. Bartsch, M. Boersma, H.-D. Franke, J. Freund, C. Gebühr, G. Gerdts, K. Stockmann, A. Wichels, Helgoland roads, North Sea: 45 years of change. *Estuaries Coasts* **33**, 295–310 (2010). doi:10.1007/s12237-009-9228-y

5. M. Kahru, V. Brotas, M. Manzano-Sarabia, B. G. Mitchell, Are phytoplankton blooms occurring earlier in the Arctic? *Glob. Change Biol.* **17**, 1733–1739 (2011). doi:10.1111/j.1365-2486.2010.02312.x

6. M. Edwards, A. J. Richardson, Impact of climate change on marine pelagic phenology and trophic mismatch. *Nature* **430**, 881–884 (2004). Medline doi:10.1038/nature02808

7. A. McQuatters-Gollop, P. C. Reid, M. Edwards, P. H. Burkill, C. Castellani, S. Batten, W. Gieskes, D. Beare, R. R. Bidigare, E. Head, R. Johnson, M. Kahru, J. A. Koslow, A. Pena, Is there a decline in marine phytoplankton? *Nature* **472**, E6–E7, discussion E8–E9 (2011). Medline doi:10.1038/nature09950

8. W. W. Gregg, C. S. Rousseaux, Decadal trends in global pelagic ocean chlorophyll: A new assessment integrating multiple satellites, in situ data, and models. *J. Geophys. Res. Oceans* **119**, 5921–5933 (2014). Medline doi:10.1002/2014JC010158

9. D. G. Boyce, M. Dowd, M. R. Lewis, B. Worm, Estimating global chlorophyll changes over the past century. *Prog. Oceanogr.* **122**, 163–173 (2014). doi:10.1016/j.pocean.2014.01.004

10. D. A. Siegel, M. J. Behrenfeld, S. Maritorena, C. R. McClain, D. Antoine, S. W. Bailey, P. S. Bontempi, E. S. Boss, H. M. Dierssen, S. C. Doney, R. E. Eplee Jr., R. H. Evans, G. C. Feldman, E. Fields, B. A. Franz, N. A. Kuring, C. Mengelt, N. B. Nelson, F. S. Patt, W. D. Robinson, J. L. Sarmiento, C. M. Swan, P. J. Werdell, T. K. Westberry, J. G. Wilding, J. A. Yoder, Regional to global assessments of phytoplankton dynamics from the SeaWiFS mission. *Remote Sens. Environ.* **135**, 77–91 (2013). doi:10.1016/j.rse.2013.03.025

11. R. J. Olson, A. A. Shalapyonok, H. M. Sosik, An automated submersible flow cytometer for analyzing pico- and nanophytoplankton: FlowCytobot. *Deep Sea Res. Part I Oceanogr. Res. Pap.* **50**, 301–315 (2003). doi:10.1016/S0967-0637(03)00003-7

12. J. B. Waterbury, S. W. Watson, F. W. Valois, D. G. Franks, Biological and ecological characterization of the marine unicellular cyanobacterium *Synechococcus*. *Can. Bull. Fish. Aquat. Sci.* **214**, 71–120 (1986).

13. S. W. Nixon, S. Granger, B. A. Buckley, M. Lamont, B. Rowell, A one hundred and seventeen year coastal water temperature record from Woods Hole, Massachusetts. *Estuaries* **27**, 397–404 (2004). doi:10.1007/BF02803532

14. N. S. R. Agawin, C. M. Duarte, S. Agusti, Growth and abundance of *Synechococcus* sp. in a Mediterranean Bay: Seasonality and relationship with temperature. *Mar. Ecol. Prog. Ser.* **170**, 45–53 (1998). doi:10.3354/meps170045

15. W. K. W. Li, Annual average abundance of heterotrophic bacteria and *Synechococcus* in surface ocean waters. *Limnol. Oceanogr.* **43**, 1746–1753 (1998). doi:10.4319/lo.1998.43.7.1746

16. A.-Y. Tsai, K.-P. Chiang, J. Chang, G.-C. Gong, Seasonal variations in trophic dynamics of nanoflagellates and picoplankton in coastal waters of the western subtropical Pacific Ocean. *Aquat. Microb. Ecol.* **51**, 263–274 (2008). doi:10.3354/ame01196

17. K. R. Hunter-Cevera, M. G. Neubert, A. R. Solow, R. J. Olson, A. Shalapyonok, H. M. Sosik, Diel size distributions reveal seasonal growth dynamics of a coastal phytoplankter. *Proc. Natl. Acad. Sci. U.S.A.* **111**, 9852–9857 (2014). Medline doi:10.1073/pnas.1321421111

18. W. K. W. Li, W. G. Harrison, E. J. H. Head, Coherent assembly of phytoplankton communities in diverse temperate ocean ecosystems. *Proc. R. Soc. London Ser. B* **273**, 1953–1960 (2006). Medline doi:10.1098/rspb.2006.3529

19. L. R. Moore, R. Goericke, S. W. Chisholm, Comparative physiology of *Synechococcus* and *Prochlorococcus*: Influence of light and temperature on growth, pigments, fluorescence and absorptive properties. *Mar. Ecol. Prog. Ser.* **116**, 259–275 (1995). doi:10.3354/meps116259

20. J. Pittera, F. Humily, M. Thorel, D. Grulois, L. Garczarek, C. Six, Connecting thermal physiology and latitudinal niche partitioning in marine *Synechococcus*. *ISME J.* **8**, 1221–1236 (2014). Medline doi:10.1038/ismej.2013.228

21. M. R. Landry, R. P. Hassett, Estimating the grazing impact of marine micro-zooplankton. *Mar. Biol.* **67**, 283–288 (1982). doi:10.1007/BF00397668

22. R. E. McDuff, S. W. Chisholm, The calculation of in situ growth rates of phytoplankton populations from fractions of cells undergoing mitosis: A clarification. *Limnol. Oceanogr.* **27**, 783–788 (1982). doi:10.4319/lo.1982.27.4.0783

23. M. Dugenne, M. Thyssen, D. Nerini, C. Mante, J. C. Poggiale, N. Garcia, F. Garcia, G. J. Grégori, Consequence of a sudden wind event on the dynamics of a coastal phytoplankton community: An insight into specific population growth rates using a single cell high frequency approach. *Front. Microbiol.* **5**, 485 (2014). Medline doi:10.3389/fmicb.2014.00485

24. F. Ribalet, J. Swalwell, S. Clayton, V. Jiménez, S. Sudek, Y. Lin, Z. I. Johnson, A. Z. Worden, E. V. Armbrust, Light-driven synchrony of *Prochlorococcus* growth and mortality in the subtropical Pacific gyre. *Proc. Natl. Acad. Sci. U.S.A.* **112**, 8008–8012 (2015). Medline doi:10.1073/pnas.1424279112

25. A. Calbet, M. R. Landry, Phytoplankton growth, microzooplankton grazing, and carbon cycling in marine systems. *Limnol. Oceanogr.* **49**, 51–57 (2004). doi:10.4319/lo.2004.49.1.0051

26. K. R. Hunter-Cevera, thesis, Massachusetts Institute of Technology and Woods Hole Oceanographic Institution (2014).

27. K. R. Hunter-Cevera, A. F. Post, E. E. Peacock, H. M. Sosik, Diversity of *Synechococcus* at the Martha's Vineyard Coastal Observatory: Insights from culture isolations, clone libraries, and flow cytometry. *Microb. Ecol.* **71**, 276–289 (2016). Medline doi:10.1007/s00248-015-0644-1

28. A. Fischer, E. Moberg, H. Alexander, E. Brownlee, K. Hunter-Cevera, K. Pitz, S. Rosengard, H. Sosik, Sixty years of Sverdrup: A retrospective of progress in the study of phytoplankton blooms. *Oceanography* **27**, 222–235 (2014). doi:10.5670/oceanog.2014.26

29. M. J. Behrenfeld, E. S. Boss, Resurrecting the ecological underpinnings of ocean plankton blooms. *Annu. Rev. Mar. Sci.* **6**, 167–194 (2014). Medline doi:10.1146/annurev-marine-052913-021325

30. K. Banse, in *Primary Productivity and Biogeochemical Cycles in the Sea*, P. G. Falkowski, A. D. Woodhead, K. Vivirito, Eds. (Springer, 1992), pp. 409–440.

31. E. E. Peacock, R. J. Olson, H. M. Sosik, Parasitic infection of the diatom *Guinardia delicatula*, a recurrent and ecologically important phenomenon on the New England Shelf. *Mar. Ecol. Prog. Ser.* **503**, 1–10 (2014). doi:10.3354/meps10784

32. H. M. Sosik, R. J. Olson, M. G. Neubert, A. Shalapyonok, A. R. Solow, Growth rates of coastal phytoplankton from time-series measurements with a submersible flow cytometer. *Limnol. Oceanogr.* **48**, 1756–1765 (2003). doi:10.4319/lo.2003.48.5.1756

33. S. R. Brody, M. S. Lozier, J. P. Dunne, A comparison of methods to determine phytoplankton bloom initiation. *J. Geophys. Res. Oceans* **118**, 2345–2357 (2013). doi:10.1002/jgrc.20167